

# Accurate interchannel pitch control in graded-index circular-core polymer parallel optical waveguide using the Mosquito method

Ryota Kinoshita,<sup>1</sup> Daisuke Suganuma,<sup>1</sup> and Takaaki Ishigure<sup>2,\*</sup>

<sup>1</sup>Graduate School of Science and Technology, Keio University, 3-14-1 Hiyoshi, Kohoku-ku, Yokohama, 223-8522, Japan

<sup>2</sup>Faculty of Science and Technology, Keio University, 3-14-1 Hiyoshi, Kohoku-ku, Yokohama, 223-8522, Japan  
[\\*ishigure@appi.keio.ac.jp](mailto:ishigure@appi.keio.ac.jp)

**Abstract:** We successfully fabricate polymer optical waveguides with graded-index (GI) circular cores whose diameter and interchannel pitch are accurately controlled using the Mosquito method: GI-core waveguides with 250-, 125- and 62.5- $\mu\text{m}$  pitches are successfully obtained. The Mosquito method utilizing a microdispenser is a very simple technique for fabricating GI-circular-core polymer optical waveguides. The accurately controlled pitch is confirmed by a high connectivity with a commercially available multimode fiber (MMF) ribbon with a 125- $\mu\text{m}$  pitch. Furthermore, by inserting the waveguide between two 12-channel MMF ribbons, we experimentally demonstrate 11.3 Gbps  $\times$  12 Ch. parallel signal transmission through a GI-core waveguide with a 125- $\mu\text{m}$  pitch for the first time to the best of our knowledge.

©2014 Optical Society of America

**OCIS codes:** (200.4650) Optical interconnects; (230.7370) Waveguides; (130.5460) Polymer waveguides.

---

## References and links

1. M. A. Taubenblatt, "Optical interconnects for high performance computing," in *Technical Digest of Opt. Fiber Commun. Conf.*, OThH3, Los Angeles, California, USA., 6–11 Mar., 2011.
2. R. C. A. Pitwon, K. Wang, J. Graham-Jones, I. Papakonstantinou, H. Baghsiahi, B. J. Offrein, R. Dangel, D. Milward, and D. R. Selviah, "FirstLight: Pluggable optical interconnect technologies for polymeric electro-optical printed circuit boards in data centers," *J. Lightwave Technol.* **30**(21), 3316–3329 (2012).
3. F. E. Doany, C. L. Schow, B. G. Lee, R. A. Budd, C. W. Baks, C. K. Tsang, J. U. Knickerbocker, R. Dangel, B. Chan, H. Lin, C. Carver, J. Haung, J. Berry, D. Bajkowski, F. Libsch, and J. A. Kash, "Terabit/s-class optical PCB links incorporating 360-Gb/s bidirectional 850 nm parallel optical transceivers," *J. Lightwave Technol.* **30**, 560–571 (2012).
4. Y. Matsuoka, D. Kawamura, K. Adachi, Y. Lee, S. Hamamura, T. Takai, T. Shibata, H. Masuda, N. Chujo, and T. Sugawara, "20-Gb/s/ch High-speed low-power 1-Tb/s multilayer optical printed circuit board with lens-integrated optical devices and CMOS IC," *IEEE Photonics Technol. Lett.* **23**(18), 1352–1354 (2011).
5. Y. Takeyoshi and T. Ishigure, "High-density 2 $\times$ 4 channel polymer optical waveguide with graded-index circular cores," *J. Lightwave Technol.* **27**(14), 2852–2861 (2009).
6. T. Ishigure and Y. Takeyoshi, "Polymer waveguide with 4-channel graded-index circular cores for parallel optical interconnects," *Opt. Express* **15**(9), 5843–5850 (2007).
7. K. Soma and T. Ishigure, "Fabrication of a graded-index circular-core polymer parallel optical waveguide using a microdispenser for a high-density optical printed circuit board," *IEEE J. Sel. Top. Quantum Electron.* **19**(2), 3600310 (2013).
8. T. Kosugi and T. Ishigure, "Polymer parallel optical waveguide with graded-index rectangular cores and its dispersion analysis," *Opt. Express* **17**(18), 15959–15968 (2009).
9. [http://www.musashi-engineering.co.jp/e.cn.hp.transer.com/products/115\\_3-4-1-12.html](http://www.musashi-engineering.co.jp/e.cn.hp.transer.com/products/115_3-4-1-12.html)
10. T. I. R. Ishiguro, H. Uno, and H.-H. Hsu, "Maximum channel density in multimode optical waveguides for parallel interconnections," in *Proceeding of 61st Electron. Compon. Technol. Conf.* (Institute of Electrical and Electronics Engineers, New York, 2011), pp. 1847–1851.
11. R. Kinoshita, K. Moriya, K. Choki, and T. Ishigure, "Polymer optical waveguides with GI and W-shaped cores for high-bandwidth-density on-board interconnects," *J. Lightwave Technol.* **31**(24), 4004–4015 (2013).
12. H. Uno and T. Ishigure, "GI-core polymer parallel optical waveguide with high-loss, carbon-black-doped cladding for extra low inter-channel crosstalk," *Opt. Express* **19**(11), 10931–10939 (2011).
13. H. Nasu, "Short-reach optical interconnects employing high density parallel-optical modules," *J. Sel. Top. Quantum Electron.* **16**(5), 1337–1346 (2010).

14. S. Yakabe, T. Ishigure, and S. Nakagawa, "Link power budget advantage of GI-core polymer optical waveguide for waveguide-based optical link," in *Technical Digest of Opt. Fiber Commun. Conf.*, OM2J.3, Los Angeles, California, USA., 4–9, Mar., 2012.
- 

## 1. Introduction

For the further advancement of high-performance computers (HPCs), optical interconnects are highly anticipated because of the capability of high-bandwidth-density wirings with low power consumption [1]. In current HPC systems, multimode fiber (MMF) links are already installed for board-to-board interconnects, so optical wirings for chip-to-chip interconnects are the next technology issue [2]. In particular, optical printed circuit boards (O-PCBs) incorporated with multimode polymer optical waveguides are currently drawing much attention [3], because multimode polymer optical waveguides are easily processed for mounting on boards and suitable for high-density wirings.

Here, an interchannel pitch of 250  $\mu\text{m}$  is widely adopted to polymer optical waveguides [4] and other components for parallel optical links such as fiber ribbons, vertical cavity surface emitting laser (VCSEL)-arrays, and photodiode (PD)-arrays. Meanwhile, in order to realize higher-density wirings, recently, narrower pitches such as 125- and even 62.5- $\mu\text{m}$  are drawing much attention [5]. For such a high-density channel alignment, we have proposed to introduce graded-index (GI) cores into polymer optical waveguides because GI-cores exhibit excellent optical characteristics compared to the conventional step-index (SI)-cores, such as low-propagation loss, low interchannel crosstalk, high bandwidth, and high coupling efficiency with MMFs, VCSELs and photo detectors (PDs) [6]-[8].

For fabricating GI-“circular”-core polymer waveguides, we developed the Mosquito method that utilizes a microdispenser for the first time in [7]. The Mosquito method allows us to simplify the fabrication of polymer optical waveguides, since it no longer needs photo-masks, large-scale UV exposure apparatus, and any chemical etching processes, even in the case when several tens of centimeters long waveguides are fabricated. On the other hand, the controllability of the core size and inter-core pitch has been an issue in this technique compared to the conventional photo-lithography method. This is because, in the Mosquito method, a liquid-state core monomer is just dispensed also *within* a “liquid-state” cladding monomer with scanning a needle for dispensing: liquid flow caused by the needle scan could devastate the alignment of the cores. In the parallel optical waveguides, even a small pitch deviation could lead to a large coupling loss between the waveguides and other optical components. Therefore, in this paper, we focus on the accurate control of the physical dimension of GI-core polymer waveguides: particularly we experimentally demonstrate that the inter-core pitch is precisely controlled to 62.5-, 125- and 250- $\mu\text{m}$  with a deviation of only a few micrometers.

## 2. Mosquito method

In the Mosquito method, an air-pulse type microdispenser system (Musashi Engineering, Inc., dispenser: ML-808FXcom, desk-top robot: SHOT Master 300DS) is used.

The Mosquito method we proposed in [7] is illustrated in Fig. 1(a). In this paper, UV curable silicone resins (FX-W712 for core: the monomer viscosity is 12,000 cPs, FX-W713 for cladding: the monomer viscosity is 10,000 cPs supplied by ADEKA Corporation) are used. First, FX-W713 is coated on a substrate. Next, FX-W712 is dispensed from a needle attached to a syringe. Here, the needle tip remains inserted in the cladding monomer while dispensing the core monomer, as shown in Fig. 1(a), and the desk-top robot scans the needle horizontally to form a circular-shaped core. Finally, both the core and cladding are cured under UV exposure followed by post-baking at 100  $^{\circ}\text{C}$  to obtain a waveguide.

Since FX-W712 and FX-W713 are miscible, these monomers slightly diffuse into each other after the core is dispensed, resulting in the formation of a concentration distribution, as shown in Fig. 1(b). The curing reaction turns these monomers into a three-dimensionally cross-linked copolymer. Therefore, the concentration distribution of the monomers is fixed, and a refractive index profile is formed in the core. Hence, the index profile is quite stable

even at higher temperatures due to the three-dimensionally cross-linked structure, compared to the dopant-based GI-core polymer waveguides we previously reported [5, 6, 8].

In our initial investigation on the viability of the Mosquito method, we focused on the parameters influencing on the core diameter, in particular the needle scan velocity, the dispensing pressure, and the needle inner diameter. It was experimentally confirmed that the core diameters could be controlled with a deviation of  $\pm 5\%$  by fixing the above parameters. Details of these parameter settings are reported in [7] with the data of obtained core diameters and index profiles.

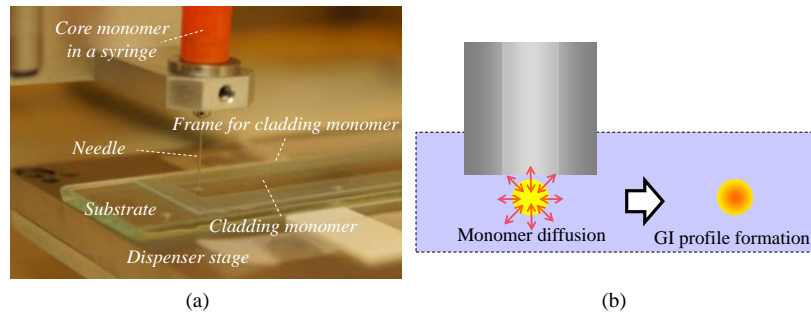


Fig. 1. (a) The fabrication process of the Mosquito method (Media 1). (b) Formation of GI refractive index profile by the monomer diffusion.

### 3. Fabrication of polymer parallel optical waveguides

#### 3.1 Pitch control method and optical evaluation method of pitch

The parallel cores in the waveguides fabricated by the Mosquito method are formed by repetitive parallel scans of the needle. In this parallel scan procedure, the position accuracy of the needle inserted in the monomer largely depends on the desk-top robot: the precision of the needle position is specified as  $\pm 5 \mu\text{m}$  [9], while the position accuracy in the vertical direction is determined by the desk-top robot: the minimum depth controllability is  $1 \mu\text{m}$ . Actually, we already succeeded in fabricating GI-core polymer optical waveguides with a  $250\text{-}\mu\text{m}$  pitch with a  $\pm 10\%$  deviation in our previous report [7]. Here, the  $10\%$  deviation of the pitch in the waveguide we previously reported corresponds to  $25\text{-}\mu\text{m}$ . Such a large deviation was observed because the needle-scan program of the desk-top robot was not optimized for pitch control. However, recent trends of polymer waveguides for optical printed circuit boards (O-PCBs) are in high-density channel alignment, which means the pitch is reduced from a traditional standard value of  $250 \mu\text{m}$  to  $125$  and  $62.5 \mu\text{m}$ . Here, since the needle outer diameter (about  $350 \mu\text{m}$ ) for forming the  $40\text{-}\mu\text{m}$  cores is much larger than the desired pitch, it is a concern that the core dispensed prior could be disturbed by the next core scans. However, we demonstrate in the following section that the Mosquito method is capable of fabricating polymer optical waveguides with a pitch remarkably smaller than the outer needle diameter.

The pitches of the fabricated waveguides are measured using an optical evaluation method as follows: A  $50\text{-}\mu\text{m}\varnothing$  GI-MMF is butt coupled to one end of the waveguide under test, while the other end is coupled to an optical power meter (ANDO AQ-2140 & AX-2741) whose active area is large enough to detect the output light from any one of 40 cores aligned in parallel. After the GI-MMF probe is actively aligned to the edge core of the waveguide, the GI-MMF probe scans horizontally with a step of  $1 \mu\text{m}$ . Then, the output power variation is plotted with respect to position. When the core of the GI-MMF is perfectly aligned to a particular core of the waveguide, the output power shows a strong peak since the coupling efficiency is maximized. This peak position is defined as the waveguide core position, and thus we can determine the pitch from the plot by calculating the distances between adjacent peaks. In order to discuss the pitch controllability, more than 10 values of pitch in a

waveguide are calculated, and then, the average value with the standard deviation is indicated in the results in the following sections.

### 3.2 250- $\mu\text{m}$ pitch waveguide

Currently, typical multimode polymer optical waveguides have had a physical dimension of  $50 \times 50 \mu\text{m}$  core size with 250- $\mu\text{m}$  pitch (SI square core) [4]. Meanwhile, in order to form a 50- $\mu\text{m}$  core using the Mosquito method, we use a needle with a 150- $\mu\text{m}$  inner diameter (an outer diameter is 350  $\mu\text{m}$ ); 24-mm/s scan velocity and 250-kPa dispensing pressure are found to be appropriate conditions. In the desk-top robot program, the needle tip (bottom) is set to have a 200- $\mu\text{m}$  height from the upper surface of the substrate before starting the needle scan, so that the cladding polymer layer is coated on the substrate with a sufficient thickness (approximately 500- $\mu\text{m}$  thick or more).

First, when the pitch is set to be 250  $\mu\text{m}$ , a cross-sectional photograph of a 5-cm long 12-Ch. GI-core waveguide fabricated is shown in Fig. 2. Although we already succeeded in fabricating GI-core polymer optical waveguides with a 250- $\mu\text{m}$  pitch [7], the dispensing conditions were adjusted not for the pitch control but for controlling the core shape and diameter. Therefore, the pitch with a  $\pm 10\%$  deviation was obtained as mentioned above. In contrast, in this paper, we optimize the needle-scan program of the desk-top robot by focusing on controlling the pitch while maintaining the dispensing conditions found in [7]. In this case, the outer *radius* of the needle is 175  $\mu\text{m}$ , which is shorter than the pre-set pitch of 250  $\mu\text{m}$ . Therefore, it is less likely that the disturbance in the parallel core alignment is due to repetitive needle scans. In fact, the pitch is controlled to  $250.7 \pm 5.2 \mu\text{m}$ . The average value of the pitch is approximately the pre-set value. On the other hand, the standard deviation value is as large as 5.2  $\mu\text{m}$ . However, as mentioned in Section 2, the specification of the desk-top robot for the position accuracy is  $\pm 5 \mu\text{m}$ , so pitch variation could depend on the fabrication setup. Higher pitch controllability should be achieved utilizing a feed-back control of the robot with additional real-time image data processing using CCD-cameras.

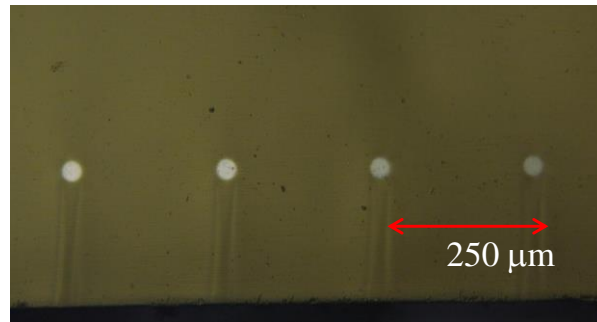


Fig. 2. A cross-sectional view of a GI-core polymer parallel optical waveguide whose pitch is controlled to 250  $\mu\text{m}$ .

### 3.3 125- and 62.5- $\mu\text{m}$ pitch waveguides

As shown in Fig. 3 on the left hand side, when a 250- $\mu\text{m}$  pitch waveguide is fabricated, the “formed core” is far apart from the side edge of the needle that is scanning the next “forming core.” On the other hand, when a 125- $\mu\text{m}$  pitch waveguide is fabricated, the formed core position overlaps the trajectory of the needle scan for the next “forming core,” as shown in Fig. 3 on the right hand side.

However, we successfully fabricate a 5-cm long waveguide with a 125- $\mu\text{m}$  pitch as shown in Fig. 4. From Fig. 4, even under a half-pitch compared to the one in Fig. 2, the circular core shape is sustained. The pitch of the waveguide shown in Fig. 4 is calculated to be  $126.7 \pm 2.6 \mu\text{m}$ . It should be noted that the pitch accuracy is higher than that of the 250- $\mu\text{m}$  pitch waveguide and the standard deviation is almost half value of the position accuracy of the robot. This result indicates that the repetitive needle scan shows little influence on the core

shape and alignment even if the needle outer radius is larger than the pitch size. The reason for the needle size showing no effects on the pitch could be that the formed cores sink in the cladding compared to the needle-tip level.

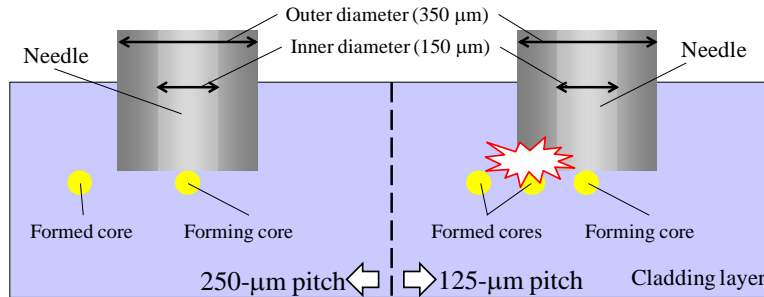


Fig. 3. Concern about fabricating the narrow-pitch waveguide.

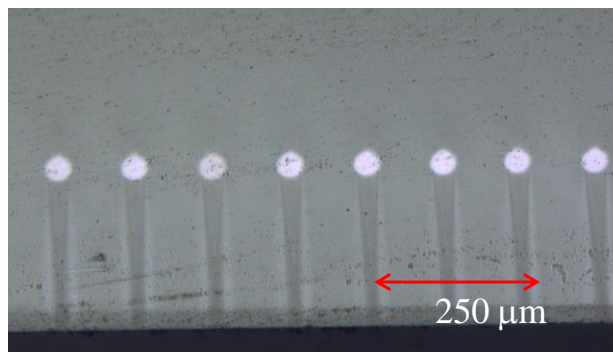
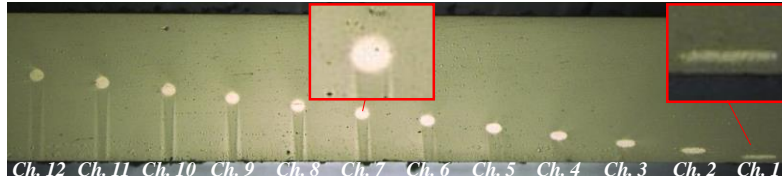


Fig. 4. A cross-sectional view of a polymer parallel optical waveguide with a 125- $\mu\text{m}$  pitch.

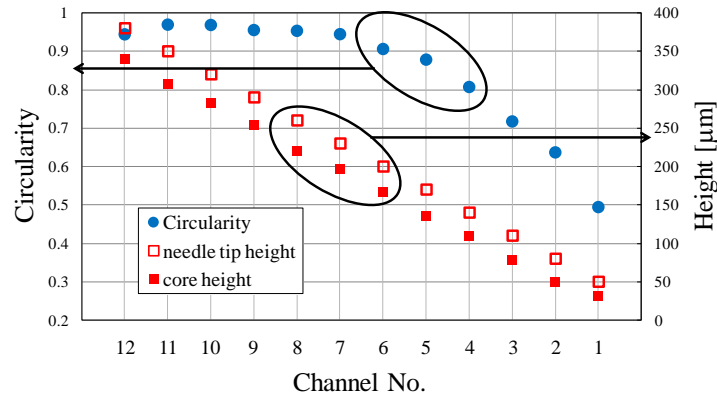
In order to confirm how the cores sink after being dispensed, we fabricate a waveguide by varying the height of the needle tip from the substrate. The same dispensing condition described above is applied to this experiment: the core size is set to 50  $\mu\text{m}$ . A cross-sectional view of the fabricated waveguide is shown in Fig. 5(a). Here, the needle-tip height of Ch. 1 in Fig. 5(a) is set to be 50  $\mu\text{m}$  from the substrate surface. The height of the needle tip is varied with a 30- $\mu\text{m}$  step from Ch. 1 to Ch. 12: The needle-tip height of Ch. 12 is set to 380  $\mu\text{m}$ . It is found that Ch. 1 is completely collapsed and elliptical cores are observed from Ch. 2 to 6. Since the dispensing condition is for a 50- $\mu\text{m}$  core, the needle-tip height for Ch. 1 is just the right size for forming a perfect circular core. Nevertheless, even other channels (Ch. 2-6) do not maintain the circular shape either. On the other hand, from Ch. 7 to 11 for which the needle-tip position ( $< 230 \mu\text{m}$ ) is high enough to maintain a perfectly circular shape, almost perfectly circular cores are formed.

In order to qualitatively evaluate the formed core shapes, we introduce a parameter of “circularity”. For the perfect circular cores, the circularity is calculated to be 1.00. The circularity of each core is determined by utilizing an image processing technique where cross-sectional photo images shown in Fig. 5 is digitized, and the number of pixels are counted to determine the circularity. For a calibration purpose, our calculation method of circularity is applied to a standard 50- $\mu\text{m}$  GI-MMF resulting in obtaining a circularity of 0.99.

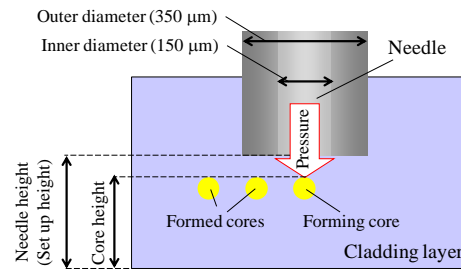
In Fig. 5(b), the calculated circularity is also plotted for all 12 channels in addition to the core-center height from the substrate surface, which is actually measured in the photo.



(a)



(b)



(c)

Fig. 5. (a) A cross-sectional view of polymer optical waveguide when the needle-tip height is varied for fabrication. (b) Relationship between the circularity and the core height from the substrate. (c) A schematic representation of the height difference between the needle tip and dispensed cores.

From Fig. 5(b), it is found that the circularity reaches to 0.95 when the needle is scanned with a height larger than 260  $\mu\text{m}$ . The maximum circularity of 0.968 is still lower than that (0.99) of a 50- $\mu\text{m}\varnothing$  GI-MMF. Therefore, optimization of the dispensing condition, particularly dispensing pressure is still required for the Mosquito method. However, even by such a simple fabrication method, almost perfectly circular cores are fabricated with high repeatability. From the results in Fig. 5, it is found that the dispensed cores are not placed just beneath the needle tip, but sink slightly in the cladding, as illustrated in Fig. 5(c), which could be due to the dispensing pressure. The average distance sunk is calculated to be 34.51  $\mu\text{m}$  from Ch. 1 to Ch. 12 in Fig. 5(b). Thus, in the case of Ch. 1 (and even Ch. 2-6), the dispensed core has no space to sink, while it is stuck between the substrate and the needle tip to be collapsed. To reduce the distance sunk, the dispensing pressure would be a key parameter.

According to the above discussion, since the fabricated waveguide pitch is independent of the needle outer diameter, we fabricate a 5-cm long waveguide with a 62.5- $\mu\text{m}$  pitch, whose cross-section is shown in Fig. 6. The pitch of this waveguide is calculated to be  $61.7 \pm 3.4$   $\mu\text{m}$ . The pitch value is slightly smaller than the pre-set value (62  $\mu\text{m}$ ). Since a position



accuracy less than  $1\ \mu\text{m}$  is not guaranteed by the desk-top robot [9], we can set the pitch with the minimum step of  $1\ \mu\text{m}$ , so that the pre-set pitch is not  $62.5\ \mu\text{m}$  but  $62\ \mu\text{m}$ . From Fig. 6, we confirm a high pitch uniformity even for a pitch as narrow as  $62.5\ \mu\text{m}$ . Thus,  $50\text{-}\mu\text{m}\varnothing$  circular GI-core polymer parallel optical waveguides with a  $62.5\text{-}\mu\text{m}$  pitch are fabricated successfully for the first time to the best of our knowledge.

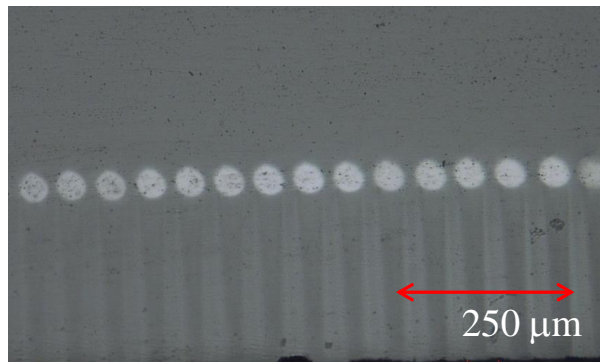


Fig. 6. A cross-sectional view of a polymer parallel optical waveguide with a  $62.5\text{-}\mu\text{m}$  pitch.

#### 4. Interchannel crosstalk

We already showed the potential of low interchannel crosstalk in GI-core waveguides even under a narrow pitch, which is due to the strong light confinement near the core center [6]. Actually, we simulated how we could decrease the interchannel pitch while keeping the interchannel crosstalk lower than  $-20\ \text{dB}$  for GI cores and then we theoretically confirmed that GI-core waveguides would be suitable for high-density optical wirings [10].

Furthermore, we also experimentally compared the interchannel crosstalk of GI-square-core waveguides with different pitches:  $62.5$ ,  $125$  and  $250\ \mu\text{m}$  (the core size is  $40 \times 40\ \mu\text{m}$  supplied by Sumitomo Bakelite Co., Ltd.) in [11]. Here, we showed that the crosstalk values almost exponentially decreased with respect to the inter-core distance, and that the slope was steeper with decreasing the pitch size. That means the crosstalk from the nearest cores dominates, and the crosstalk from the distant cores are less likely to suffer the signal integrity.

In this paper, we measure the interchannel crosstalk of GI-circular-core polymer waveguides fabricated using the Mosquito method and then, compare the pitch and core shape dependences of the crosstalk. The interchannel crosstalk is measured using the setup schematically shown in Fig. 7, which is the same as that used in [11]. First, we excite one core of the waveguide via a  $1\text{-m}$  long,  $50\text{-}\mu\text{m}\varnothing$  GI-MMF probe and measure the output power from the excited core using another  $50\text{-}\mu\text{m}\varnothing$  GI-MMF probe. Next, as shown in Fig. 7, the detection probe is scanned horizontally with a step of  $1\ \mu\text{m}$  in order to detect the output power from the other cores, as well as the output from the cladding area.

The measured results of the interchannel crosstalk are shown in Fig. 8(a). The optical power leaked from the excited core remains in the cladding and then recouples to the propagating modes in other cores as crosstalk [12]. Therefore, the crosstalk values from the cladding between the cores are large. From Fig. 8(a), the crosstalk values to the nearest channel are found to be  $-27\ \text{dB}$ ,  $-31\ \text{dB}$ , and  $-39\ \text{dB}$  for  $62.5\text{-}$ ,  $125\text{-}$ , and  $250\text{-}\mu\text{m}$  pitch GI-circular-core waveguides, respectively, which are lower than the values of the GI-square-core waveguides we measured previously ( $-21\ \text{dB}$ ,  $-26\ \text{dB}$  and  $-27\ \text{dB}$  for the corresponding pitches) [11]. The Mosquito method allows us to obtain GI-circular core waveguides with sufficiently low interchannel crosstalk: the crosstalk from the nearest core is as low as  $-30\ \text{dB}$  except for the narrowest pitch ( $62.5\ \mu\text{m}$ ) sample. Even in the case of the  $62.5\text{-}\mu\text{m}$  pitch sample, the crosstalk is lower than  $-25\ \text{dB}$ .

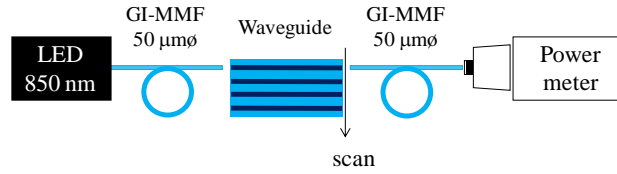


Fig. 7. Measurement setup for crosstalk characterization.

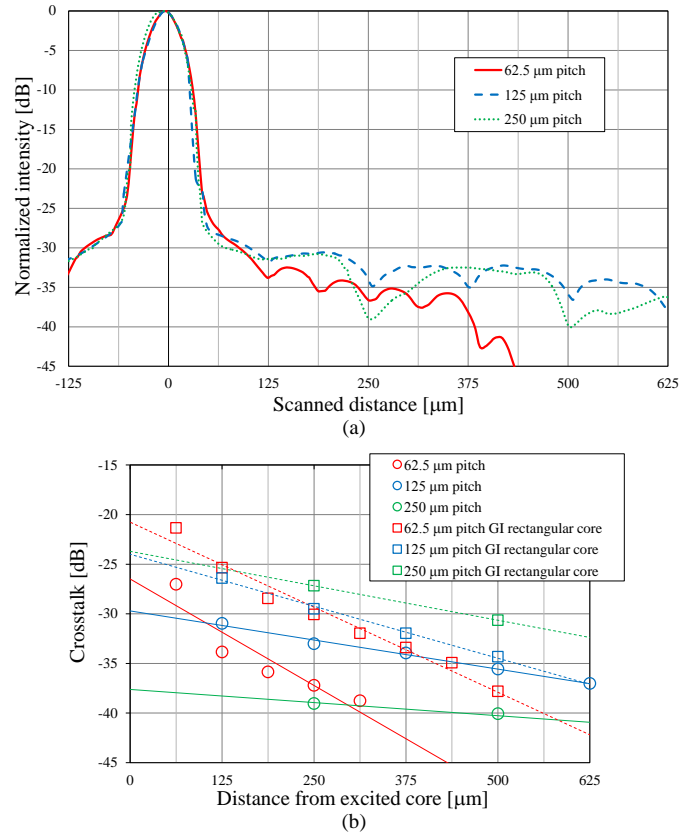


Fig. 8. (a) Interchannel crosstalk in GI-core waveguides with 250-, 125- and 62.5- $\mu\text{m}$  pitches excited via a 50- $\mu\text{m}$  GI-MMF. (b) Relationships between the interchannel crosstalk value and the inter-core distance.

In actual optical links, the accumulated crosstalk from all the cores could deteriorate the signal integrity, because parallel signals propagate through all the channels in the waveguides simultaneously. Hence, we focus on the relationship between the crosstalk value and the interchannel distance. In Fig. 8(b), the results of the fabricated waveguides using the Mosquito method are plotted with the previous results of GI-square-core waveguides. In the case of the GI-“circular”-cores (circle plots), the crosstalk values also exponentially decrease with increasing the interchannel distance: From the best-fit lines (solid lines), the slope values are found to be  $-0.005 \text{ dB}/\mu\text{m}$ ,  $-0.012 \text{ dB}/\mu\text{m}$  and  $-0.043 \text{ dB}/\mu\text{m}$  for the 250-, 125- and 62.5- $\mu\text{m}$  pitch waveguides, respectively. Meanwhile, the GI-square-core waveguides fabricated by the photo addressing method with 250, 125 and 62.5  $\mu\text{m}$  pitches show the crosstalk slope values of  $-0.014 \text{ dB}/\mu\text{m}$ ,  $-0.022 \text{ dB}/\mu\text{m}$  and  $-0.034 \text{ dB}/\mu\text{m}$  as shown in Fig. 8(b) as broken lines. The crosstalk slope is steeper with decreasing the pitch, which is the same tendency as those of GI-square-core waveguides. Therefore, the influence from the distant core on the crosstalk would decrease while the crosstalk to the nearest channel would be high in the



narrow-pitch waveguides, and we find in Fig. 8(b) that forming GI-circular-cores could decrease the dominant crosstalk from the nearest cores.

The 250- and 125- $\mu\text{m}$  pitch square-core waveguides show steeper crosstalk slopes compared to the circular core waveguides with the same pitches. Contrastingly, the crosstalk in the 62.5- $\mu\text{m}$  pitch circular-core waveguide rapidly decreases with the inter-core distance, compared to the square-core samples. What we would like to emphasize here is that the circular-core waveguides always show lower crosstalk than the square-core waveguides independent of pitch. This implies that the nearest-core crosstalk values are low. The lower crosstalk in the GI-circular cores than the square counterparts could be attributed to the thick cladding: low optical power confined in the thick cladding could decrease the crosstalk. We already discussed the optical power in the cladding and showed that optical power removal from the cladding is effective for decreasing the interchannel crosstalk [10, 11]. Therefore, the effect of the cladding thickness on the crosstalk will be reported elsewhere.

## 5. Multi-channel operation

In the above sections, the fabricated waveguides are evaluated by launching one of the multiple cores. However, in actual optical links, parallel multiple cores need to be operated simultaneously. Hence, the optical properties of the waveguides should be discussed under the conditions of all channels operating simultaneously. In this paper, the connectivity of the waveguide with a commercially available MMF ribbon is investigated, by which we show the uniformity of the multiple cores: propagation loss and pitch uniformity. For the connectivity measurement, the waveguide under test is inserted into two MMF ribbons. First, the waveguide with a 125- $\mu\text{m}$  pitch, shown in Fig. 4 is butt-coupled to a 1-m long, 12-Ch., 50- $\mu\text{m}$  GI-MMF ribbon with the same pitch (supplied by Furukawa Electric Co., Ltd.) whose end is terminated with an MT connector, as shown in the experimental setup illustrated in Fig. 9. The interchannel pitch of the fiber ribbon was measured using the method shown in 3.1 to obtain  $125.0 \pm 0.9 \mu\text{m}$ . Since each channel of the MMF ribbon is independently connected to twelve different VCSEL sources, not only all the channels but also the desired channels of the waveguides are selectively excited.

First, a near-field pattern of the 125- $\mu\text{m}$  pitch waveguide is shown in Fig. 10, where all the 12 cores are excited. From Fig. 10, we confirm sufficiently high output power from all the 12-Ch. cores. Next, we also evaluate the connectivity between the MMF ribbon and the 62.5- $\mu\text{m}$  pitch waveguide shown in Fig. 6. Since only the GI-MMF ribbon with a 125- $\mu\text{m}$  pitch is available, the GI-MMF ribbon excites every other core of the 62.5- $\mu\text{m}$  pitch waveguide. In Table 1, the insertion losses are indicated, which are measured by accurately aligning a 50- $\mu\text{m}$  GI-MMF probe instead of the Near-Field Pattern (NFP) camera in Fig. 9. In Table 1, Ch. 1, 2, 3, ..., 10, 11, and 12 of the "MMF Ribbon Channel No." correspond to Ch. 1, 2, 3, ..., 10, 11, and 12 in the 125- $\mu\text{m}$  pitch waveguide, and to Ch. 2, 4, 6, ..., 20, 22, and 24 in the 62.5- $\mu\text{m}$  pitch waveguide.

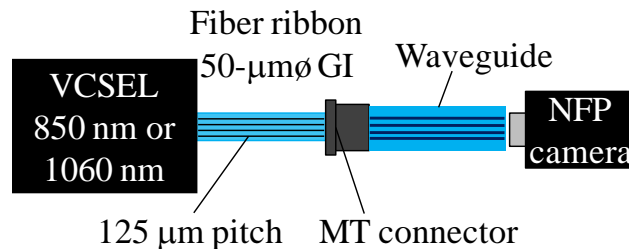


Fig. 9. Experimental set up of parallel channel operation of a waveguide.

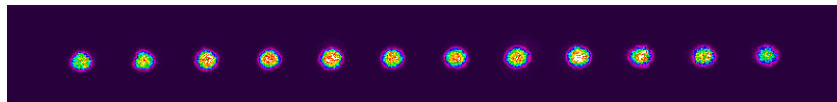


Fig. 10. A near-field pattern of waveguide when 12-Ch. cores are excited.

**Table 1. Insertion Losses of Waveguides with 125- and 62.5- $\mu\text{m}$  Pitches at 1060-nm Wavelength [dB]**

MMF Ribbon Channel No.	1	2	3	4	5	6	7	8	9	10	11	12
125- $\mu\text{m}$ pitch	3.60	4.03	3.02	2.03	2.43	2.47	2.42	2.03	2.20	2.73	2.44	3.24
62.5- $\mu\text{m}$ pitch	3.85	3.66	2.35	2.88	3.27	2.85	3.89	2.72	6.69	2.38	3.35	2.13

For the insertion loss measurement, 1060-nm VCSELs are used as a preparation of high-speed data transmission experiment shown in the next part. A 2-dB variation of the insertion loss (from 2.03 to 4.03 dB) is observed in the 125- $\mu\text{m}$  pitch waveguide. Similar variation is also observed in the 62.5- $\mu\text{m}$  pitch waveguide, except for Ch. 9. Even for the core exhibiting the highest insertion loss, the output power is high enough for a high-speed data transmission experiment: the output power from all the cores is higher than minimum sensitivity of the PD.

Therefore, using the waveguide shown in Fig. 4, we demonstrate a high-speed parallel signal transmission (11.3-Gbps  $\times$  12-Ch.) through a GI-core parallel optical waveguide for the first time, where we use parallel-optical transceivers employing 1060-nm VCSELs developed at Furukawa Electric Co., Ltd [13]. A schematic representation of the experimental setup is shown in Fig. 11 along with a photo. One end of a 50- $\mu\text{m}$  $\varnothing$  GI-MMF ribbon with a 250- $\mu\text{m}$  pitch is coupled to the transmitter, while the other end is connected via an MT connector to another MMF ribbon with a 250- $\mu\text{m}$  /125- $\mu\text{m}$  pitch conversion structure. Then, the 5-cm long polymer waveguide is butt-coupled to the MMF on the side of 125- $\mu\text{m}$  pitch (with an MT connector), as shown in Fig. 11. After propagating through the waveguide, the output lights from the cores are connected to another 125- $\mu\text{m}$  pitch GI-MMF ribbon to guide to the receiver array to measure the eye diagrams.

Table 2 summarizes the measured output power from each channel (output power from the receiver-side GI-MMF ribbon) and the insertion loss (comparison with the output power from the launching MMF ribbon). As shown in Table 2, the output power from Ch. 1 to Ch. 12 shows approximately a 3-dB variation: 1 dB higher than the insertion loss variation in Table 1. The higher insertion losses are mainly due to the coupling losses between the waveguide and the GI-MMF ribbon.

The propagation loss of the same silicone based GI-core waveguide at 1060 nm was previously measured in [7] as 0.15 dB/cm, which is slightly higher than the propagation loss at 850-nm wavelength (0.033 dB/cm) due to higher vibrational absorption loss of carbon-hydrogen bonding. However, as the total propagation loss for a 5-cm long waveguide is calculated to be 0.75 dB (0.15 dB/cm  $\times$  5 cm) at 1060 nm, the high absorption loss at 1060 nm shows a small influence on the averaged insertion loss of 2 to 4 dB shown in Table 1 for the 12 channels. Since the pitch of the waveguide is precisely controlled to be 125  $\mu\text{m}$ , an insertion loss is as low as 2 to 4 dB in all the channels.

We also evaluated the misalignment tolerance of the connection between a GI-core waveguide and a GI-MMF in [7], and it was found that even a 10- $\mu\text{m}$  misalignment caused 0.5-dB loss increment at the MMF-waveguide connections. Meanwhile, an excess loss as high as 3 to 4 dB is observed in Ch. 10 and Ch. 12 compared to Ch. 6 in Table 2. The insertion losses in Table 2 include additional 2 to 3 dB loss in all the channels compared to the loss of corresponding channels in Table 1. These excess coupling losses are probably because the dual misalignment at both ends of the waveguide. At the input end face, when misalignment is caused between the GI-MMF ribbon and the waveguide cores, high-order modes in the cores of waveguide are selectively excited, which increases the output spot size of the near-field pattern at the output end of the waveguide. Then, the insertion losses of the second connection (waveguide to another MMF ribbon) could increase. Therefore, for reducing the insertion loss variation, further accurate pitch control should be realized: a feedback method using CCDs could be one solution.

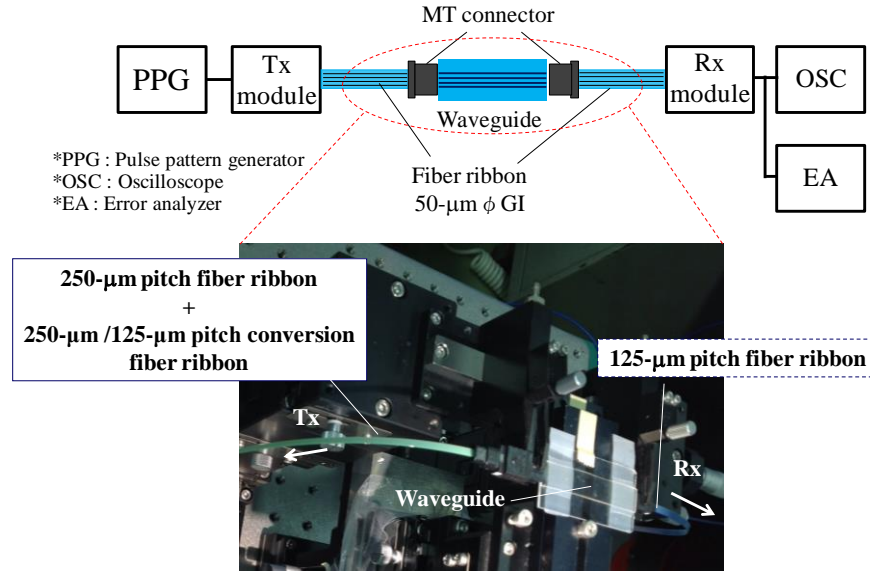


Fig. 11. Experimental setup for multiple-core operation.

**Table 2. Output Power and Insertion Loss for Link with a 5-cm Long Waveguide.**

Waveguide Channel No.	1	2	3	4	5	6	7	8	9	10	11	12
Output Power [dBm]	-6.70	-4.51	-4.15	-3.65	-3.68	-3.55	-4.37	-4.25	-6.09	-7.46	-6.94	-7.22
Insertion loss [dB]	7.15	4.98	4.87	4.44	4.12	4.17	5.09	4.96	6.92	8.12	7.17	7.51

Figure 12 shows the measured optical eye diagrams operated at after 11.3-Gbps  $2^{31}-1$  pseudo-random binary sequence (PRBS) bit-stream for each channel. In terms of a high speed serial optical transmission, we demonstrated a 25-Gbps optical link utilizing just one core in a GI polymer parallel optical waveguide in a previous work [14]. Meanwhile, the results in Fig. 12 are the first demonstration of multi-channel parallel-optical transmission in such a narrow-pitch GI-core waveguide. Since the pitch of the waveguide fabricated using the Mosquito method is accurately controlled to 125  $\mu\text{m}$ , the insertion losses are low enough in all the channels, and thus, all eye diagrams observed in Fig. 12 are clearly open.

Next, we measure bit error rate (BER) bathtub curves using the setup in Fig. 11. Here, we focus on Ch. 6 since it shows the lowest insertion loss in Table 2, and in order to check the influence of interchannel crosstalk on BER, we compare BER bathtub curve when all channels are operated to those of back-to-back, and when only Ch. 6 is operated. Measured BER bathtub curves are shown in Fig. 13. From Fig. 13, the jitter margins are 0.45 U.I. or more even with all channels operating. Meanwhile, the measured random jitter increment under all channels operation compared to single-channel operation is almost 0.05 U.I.. A slight jitter variation is also observed compared to two back-to-back patterns, as shown in Fig. 13. However, those jitter variations are caused mainly by the electric crosstalk, because the curve of back-to-back under all channel operation shows larger jitter variation than under single-channel operation. Therefore, it is confirmed that the signal deterioration due to the optical crosstalk is negligible even under a pitch as narrow as 125  $\mu\text{m}$ .

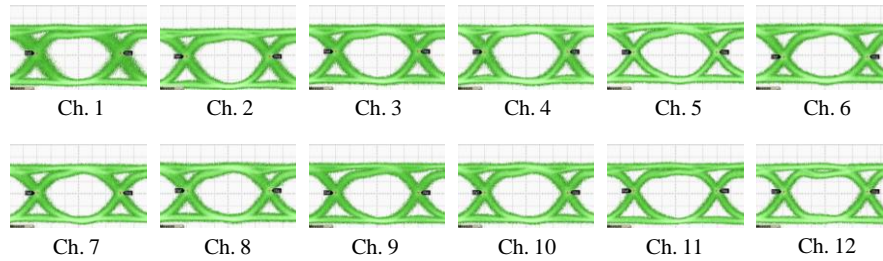


Fig. 12. Eye diagrams for 11.3 Gbps parallel-optical signals after transmitting a 5-cm long waveguide with a 125- $\mu\text{m}$  pitch.

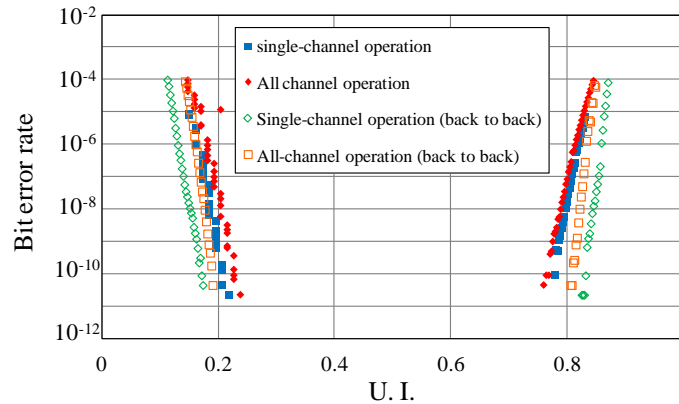


Fig. 13. Bit error rate curves for 11.3 Gbps transmission when only Ch. 6 is operated and 12 channels are operated.

## 6. Conclusion

We successfully fabricated the GI-circular-core polymer parallel optical waveguides whose interchannel pitch is accurately controlled using the Mosquito method. The waveguide pitches were measured as  $250.7 \pm 5.2$ ,  $126.7 \pm 2.6$ , and  $61.7 \pm 3.4$   $\mu\text{m}$  for the pre-set pitch of 250-, 125-, and 62.5- $\mu\text{m}$ , respectively. We also investigated the crosstalk properties of the fabricated GI-circular-core waveguides, and discussed the relationship between interchannel crosstalk and the pitch or the distance from the excited core. Because of the well-controlled pitch, the fabricated GI waveguides showed a high connectivity with a 12-Ch. GI-MMF ribbon with a 125- $\mu\text{m}$  pitch. Finally, we experimentally demonstrated 11.3 Gbps  $\times$  12 Ch. signal transmissions in the parallel 12 channels without any signal deterioration. Therefore, GI-circular-core polymer parallel optical waveguides fabricated using the Mosquito-method could pave the way for higher-bandwidth-density on-board and board-to-board optical interconnects.

## Acknowledgments

The authors would like to acknowledge Y. Ishikawa of ADEKA Corporation for supplying silicone polymer materials and for his continuous technical support to this research. In addition, the authors would like to acknowledge H. Nasu and K. Nagashima of Furukawa Electric Co., Ltd. for supplying 50- $\mu\text{m}$  GI-MMF ribbons with variable pitch size and for allowing us to use their high-speed data transmission experimental setup with continuous technical support.